Back Flips with a Hexapedal Robot

Uluç Saranli* and Daniel E. Koditschek*

Department of Electrical Engineering and Computer Science
The University of Michigan, Ann Arbor, MI 48109-2110, USA

Abstract

We report on the design and analysis of a controller which can achieve dynamical self-righting of our hexapedal robot, RHex. We present an empirically developed control procedure which works reasonably well on indoor surfaces, using a hybrid energy pumping strategy to overcome torque limitations of its actuators. Subsequent modeling and analysis yields a new controller with a much wider domain of success as well as a preliminary understanding of the necessary hybrid control strategy. Simulation results demonstrate the superiority of the improved control strategy to the first generation empirically designed controller.

1 Introduction

RHex is an autonomous hexapod robot that negotiates badly irregular terrain at speeds better than one body length per second [8]. In this paper, we report on efforts to extend RHex's present capabilities with a self-righting controller. Motivated by the successes and limitations of an empirically developed "energy pumping" scheme, we introduce a careful multi-point contact and collision model so as to derive the maximum benefit of our robot's limited power budget. A comparative simulation study suggests that the new controller will extend significantly the terrain over which the self-righting maneuver succeeds.

Recovery of correct body orientation is among the simplest of self-manipulation tasks. In cases where it is impossible for a human operator to intervene, the inability to recover from a simple fall can completely render a robot useless. Especially in outdoor environments with badly broken terrain and obstacles of various shapes and sizes, the debilitating effects of such accidents have been observed in the past [2].

RHex's morphology is roughly symmetric with respect to the horizontal plane, and allows nearly identical upside-down or right-side up operation, a solution adopted by other mobile platforms [7]. However, various scenarios such as teleoperation and vision based navigation entail a nominal orientation as a result of the accompanying instrumentation and algorithms. Under these constraints, most existing robotic designs with self-righting capabilities incorporate special kinematic structures such as long extension arms or reconfigurable wheels [6, 10]. In consequence of weight and power limitations, RHex is not equipped with such structures and must rely on its existing morphology and dynamic maneuvers to perform a flip-over.

Beyond reporting on the existing behavior and the new multiple point collision/contact model, the main contribution of the paper is a torque control strategy that maximizes the energy injected into the system, validated for now by a comparative simulation study and a second empirical study, presently in progress.

2 Flipping RHex

Our first generation flipping controller consists of a state machine, illustrated in Figure 1. Starting from a stationary position on the floor, the robot very quickly (in 0.2s) goes through two configurations (poses I and II in Figure 1), with front and middle legs successively leaving the ground. Depending on the frictional properties of the ground, these motions result in some initial kinetic energy of the body that may in some cases be sufficient to allow "escape" from the gravitational potential well of the initial configuration and fall into the other desired configuration. However, on most surfaces — gravel, grass and asphalt, but even some indoor settings such as carpet — this is not sufficient to flip the body over. Instead, the robot reaches some maximum pitch lying within the basin of the original configuration, and the robot falls back toward its initial state. Under these circumstances, the controller brings the legs back to Pose I of Figure 1 and waits for the impact of the front legs with the ground, avoiding negative work — a waste of battery energy given the familiar power-torque limitations of RHex's conventional DC motors. The impact of the front legs with

*Supported in part by DARPA/ONR Grant N00014-98-1-0747

concrete	linoleum	carpet	asphalt	grass	gravel
90%	100%	90%	100%	0%	0%

Table 1: Success rates of the first generation controller for 10 experiments each on different surfaces.

the ground in their kinematically singular configuration recovers some of the body's kinetic energy, followed by additional thrust from the middle and back legs, during the period of decompression and flight of the front leg — i.e., during a phase interval when it is possible for the legs in contact to perform positive work on the robot's mass center. Thrusting is achieved by running a high gain proportional derivative control (PD) law around a judiciously selected constant velocity leg sweep motion. The maximum pitch attained by the body increases with each bounce up until the point where collision losses are exceeded by the energy that can be be imparted by the PD controller during the leg sweep phase interval. As Table 1 suggests, this pumping strategy works very reliably on a number of common surfaces such as linoleum, smooth concrete, carpet and asphalt.

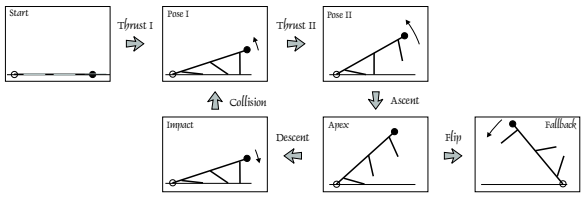

Figure 1: Sequence of states for the flipping controller

However, on many surfaces — the outdoor environments most relevant to RHex's presumed mission [1, 8] such as loose gravel, grass and soft ground — it does not perform nearly as well. To permit a reasonable degree of autonomous operation, we would like to improve on the range of conditions flipping can function. This requires a more aggressive torque generation strategy for the middle and rear legs. However, empirically, we find that driving all available legs with the maximum torque allowed by the hip motors results in the body lifting off the ground into stance mode, still in the wrong configuration. We require a strategy that can be tuned carefully enough to produce larger torques aimed specifically at pitching the body over. This requires a detailed model of the manner in which the robot can elicit ground reaction forces in consequence of hip torques operating at different body states and leg contact configurations.

3 The Planar Flipping Model

3.1 A Generic Planar Model

In this section, we describe a three degree of freedom planar model. Section 3.3 then presents the much simpler, single degree of freedom model that will be used in our algorithm design and subsequent analysis (presently in progress). Both models assume that the flipping behavior is primarily planar.

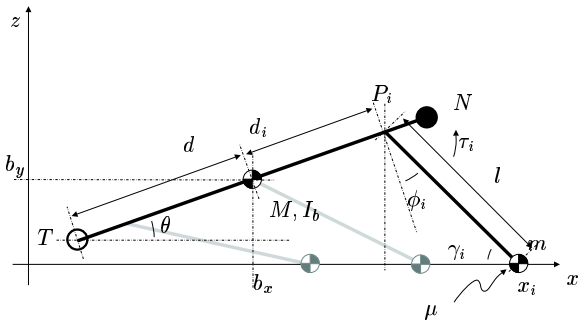

Figure 2: Simple rigid planar model of RHex

Figure 2 illustrates our unconstrained planar model. Three rigid legs with point masses m on the toes are attached to a rigid body with mass M and inertia I_b. The toe masses are only effective when the leg is touching the ground and are neglected when the leg is in flight. The attachment points of the legs are fixed, along a straight line through the center of mass. This line also defines the orientation of the body, θ, with respect to the horizontal. The body extends between the points N(nose) and T(tail), which are equidistant from the center of mass, yielding a body length of $2d$. The nose, the tail and the toes cannot penetrate the ground. We assume that the body-ground friction is infinite thereby precluding any possibility of horizontal slip of the tail and the nose. In contrast, horizontal motion of the toes along the ground is central to the behavior of interest. We model the toe ground interaction as characterized by Coulomb friction with dynamic coefficient μ and viscous friction with damping constant k_d. Table 2 summarizes the notation used throughout the paper.

3.2 Contact States and Constraints

Five binary flags, — a pair for the body end points, and a triple for the legs, denoted, respectively, as s_n, s_t, s_1, s_2, s_3 — are sufficient to encode the contact

$\mathbf{q} = [\theta, \dot{\theta}] \in T\mathcal{Q}$	System state vector
ϕ_i	Leg angle wrt the body vertical
γ_i	Leg angle wrt the horizontal (cw)
x_i	Horizontal pos. of the toe mass
$\boldsymbol{\tau} \in \mathbb{R}^3$	Hip torque control vector
$\mathcal{T}(\mathbf{q}, p)$	Set of allowable torque vectors
F_i	Vert. grnd. reaction force on toe i
d, d_i, l	Kinematic parameters
M, I_b, m	Body mass and inertia, toe mass
γ_c	Toe angle at leg-ground collision
k_r	Leg-ground coeff. of restitution

Table 2: Notation used throughout the paper.

d (m)	d_1 (m)	d_2 (m)	d_3 (m)	l (m)	M (kg)	I_b (kgm^2)	m (kg)
0.28	-0.2	0	0.2	0.12	7.5	0.18	0.1

Table 3: RHex's kinematic and dynamic parameters.

configurations of the system,

$$[(s_n, s_t), (s_1, s_2, s_3)] \in \mathcal{H}_b \times \mathcal{H}_l$$
$$\mathcal{H}_b := \{0,1\} \times \{0,1\},$$
$$\mathcal{H}_l := \{0,1\} \times \{0,1\} \times \{0,1\}.$$

For any $s \in \mathcal{H}_l$, we use s_i to denote the corresponding contact state for the i^{th} leg for $i = 1, 2, 3$. We will also find it useful to introduce a partial order on $\mathcal{H}_l$,[1]

Definition 1 *Let $p, r \in \mathcal{H}_l$. We denote by the symbol $\geq$, the following relation*

$$(p \geq r) \Leftrightarrow ((\forall i \; p_i = 0 \rightarrow r_i = 0)) \tag{1}$$

3.3 The 1DOF Planar Model

Our subsequent analysis mainly concerns configurations where the tail of the body is in contact with the ground maximizing the duration of thrust from the front legs. This also decreases the magnitude of the potential barrier or the vertical orientation and avoids losses arising from the body-ground collisions. Our controller design in Section 4 respects this constraint by proper choice of control inputs, reducing the system to only one degree of freedom: the body angle θ. By convention, we coincide the tail with the origin. The foot position and leg orientation can then be expressed as functions of θ,

$$\begin{aligned} x_i &= (d_i + d)\cos\theta + l\cos\gamma_i \\ \gamma_i &= \operatorname{asin}\left[\frac{d_i + d}{l}\sin\theta\right]. \end{aligned} \tag{2}$$

We will also find it convenient to write the leg contact constraints in functional form, $s_c : \mathcal{Q} \rightarrow \mathcal{H}_l$, with the i^{th} leg component specified as

$$s_c(\;\theta\;)_i = \begin{cases} 1 & \text{if } \sin\theta \leq l/(d + d_i) \\ 0 & \text{otherwise} \end{cases}.$$

In the sequel, we will refer to the dynamical state of the system, $\mathbf{q}$, as the *body state* and the discrete leg touchdown configuration as the *contact state*.

3.4 Continuous Dynamics

In this section, we derive the contact constraint forces and the vector field for the constrained model of Section 3.3, for a particular choice of contact state, assuming that the legs that are touching the ground as well as the tail of the body are vertically constrained in both directions (i.e. the ground reaction force can be negative as well as positive). We then present the final form of the equations of motion using the actual contact state $s_m(\mathbf{q}, \boldsymbol{\tau}) \leq s_c(\theta)$, defined in Section 3.5 to yield the continuous dynamics for our model.

Free body analysis of the body link and one of the legs in contact with the ground yields,

$$\begin{aligned} &(l\cos\gamma_i + l\bar{\mu}_i \sin\gamma_i)F_i \\ &\qquad = lma_i^x \sin\gamma_i - lmb_i^x\ddot{\theta}\sin\gamma_i - \tau_i + k_d\dot{x}_i \end{aligned} \tag{3}$$

where $\bar{\mu}_i := -\mu \; \text{sign}(\dot{x}_i)$, k_d is the frictional damping constant and $\ddot{x}_i = a_i^x - b_i^x\ddot{\theta}$ is obtained from (2).

Combined with the moment balance for the body link around the tail, instances of (3) for each leg that can reach the ground result in a linear set of equations whose solution yields the dynamics.

The number of these equations, however, varies based on the value of $s_c(\theta)$. The following presentation assumes that all the legs can reach the ground, i.e. $s_c(\theta) = [1, 1, 1]$, but the readers should note that there are 2^3 different cases for different contact states. According to the free body diagram, we may write

$$\mathbf{A}_p(\mathbf{q})\;\mathbf{v} \quad = \quad \mathbf{b}(\mathbf{q}, \boldsymbol{\tau}) \tag{4}$$

where $\mathbf{q} \in T\mathcal{Q}$, $p = [p_1, p_2, p_3] \in \mathcal{H}_l$ is an arbitrary contact state such that $p \leq s_c(\theta)$ and the arrays are specified as follows:

$$\mathbf{A}_p(\mathbf{q}) := \begin{bmatrix} f_1 & 0 & 0 & lmb_1^x \sin\gamma_1 \\ 0 & f_2 & 0 & lmb_2^x \sin\gamma_2 \\ 0 & 0 & f_3 & lmb_3^x \sin\gamma_3 \\ p_1x_1 & p_2x_2 & p_3x_3 & -(I_b + Md^2) \end{bmatrix} \tag{5}$$

[1] See [9] for a proof that (1) indeed defines a partial order.

$$\mathbf{b}(\mathbf{q},\boldsymbol{\tau}) := \begin{bmatrix} lm\ a_1^x\ \sin\gamma_1 + k_d\dot{x}_1 - \tau_1 \\ lm\ a_2^x\ \sin\gamma_2 + k_d\dot{x}_2 - \tau_2 \\ lm\ a_3^x\ \sin\gamma_3 + k_d\dot{x}_3 - \tau_3 \\ Mgd\cos\theta \end{bmatrix}$$

$$\mathbf{v} := \begin{bmatrix} F_1 & F_2 & F_3 & \ddot{\theta} \end{bmatrix}^T$$

$$f_i := l\cos\gamma_i + l\bar{\mu}_i \sin\gamma_i \ .$$

The matrix $\mathbf{A}_p(\mathbf{q})$ is always invertible in the range of operation for our controller [9]. Consequently, the solution to (4) yields the ground reaction forces on the legs as well as the vector field for the particular contact state choice p,

$$\mathbf{v}_p(\mathbf{q},\boldsymbol{\tau}) := \mathbf{A}_p(\mathbf{q})^{-1}\ \mathbf{b}(\mathbf{q},\boldsymbol{\tau}) \ . \tag{6}$$

The equations of motion use the actual contact state, $p = s_m(\mathbf{q},\boldsymbol{\tau})$, defined in Section 3.5,

$$\ddot{\theta}(\mathbf{q},\boldsymbol{\tau}) = [\ 0\ 0\ 0\ 1\ ]\ \mathbf{A}_{s_m(\mathbf{q},\boldsymbol{\tau})}(\mathbf{q})^{-1}\mathbf{b}(\mathbf{q},\boldsymbol{\tau}) \tag{7}$$

and only depends on the current body state and the torque input vector, the value of the contact state already being determined.

3.5 Hybrid Leg Contacts

Given the current state $\mathbf{q}$, we can "read off" from $s_c(\theta)$ the number of kinematically possible leg contacts so as to determine the dimension of the square array $\mathbf{A}_p(\mathbf{q})$ in (4). However, only when a specific set of torques, $\boldsymbol{\tau} \in \mathbb{R}^3$, is also imposed, can we determine the actual leg contact state according to the function, $s_m : T\mathcal{Q} \times \mathbb{R}^3 \to \mathcal{H}_l$, and complete the specification of the dynamics in (7). We now introduce maximality, which has a key role in our determination of s_m.

Definition 2 *$p \in \mathcal{H}_l$ is called* consistent *at a particular state $\mathbf{q}$ and for a given control input vector $\boldsymbol{\tau}$, denoted* $\text{cons}_{[\mathbf{q},\boldsymbol{\tau}]}(p)$*, if and only if*

$$\forall i\ (p_i = 1) \to F_i(q,\boldsymbol{\tau},p) > 0$$

Definition 3 *Let $p \in \mathcal{H}_l$ be a contact state. p is* maximal *at $[\mathbf{q},\boldsymbol{\tau}]$, denoted* $\text{maximal}_{[\mathbf{q},\boldsymbol{\tau}]}(p)$*, if and only if*

$$\text{cons}_{[\mathbf{q},\boldsymbol{\tau}]}(p) \to (\forall r \in \mathcal{H}_l\ \text{cons}_{[\mathbf{q},\boldsymbol{\tau}]}(r) \to (p \geq r)) \tag{8}$$

Lemma 1 *If $p \in \mathcal{H}_l$ is the maximal contact state at $\mathbf{q}$ for a given $\boldsymbol{\tau}$, then*

$$\forall r \in \mathcal{H}_l, (r \leq p) \to (\ddot{\theta}_r(\mathbf{q},\boldsymbol{\tau}) \leq \ddot{\theta}_p(\mathbf{q},\boldsymbol{\tau}))$$

Detailed proofs for the existence and uniqueness of the maximal contact state as well as Lemma 1 can be found in [9]. Based on these properties, the following assumption is the basis of our hybrid contact model.

A 1 *The contact state of the system is the maximal contact state for its current body state $\mathbf{q}$ and a specified control torque vector $\boldsymbol{\tau}$.*

The following algorithm hence computes the maximal and hence the actual contact state.

Algorithm 1 *(Definition of $s_m : T\mathcal{Q} \times \mathbb{R}^3 \to \mathcal{H}_l$)*
For a given state $\mathbf{q} \in T\mathcal{Q}$ and control inputs $\boldsymbol{\tau} \in \mathbb{R}^3$, this iterative algorithm determines a consistent contact state assignment which is also maximal.

1. *Start with an initial leg contact state based on the kinematic constraints, $p^0 = s_c(\theta)$.*
2. *Using (4), compute ground reaction forces $F_i(p^k)$ arising from the leg contact state p^k.*
3. *If $\forall i,\ F_i(p^k) > 0$, p_k is the actual touchdown state, stop the iterations. Otherwise, proceed with the next step.*
4. *Choose the next leg touchdown states to be considered as follows.*

$$p_i^{k+1} = \begin{cases} p_i^k & \text{if } F_i(p^k) > 0 \\ 0 & \text{otherwise} \end{cases} \quad \text{for } i = 1,2,3$$

5. *Go to step 2 with $k \leftarrow k+1$*

3.6 Leg-Ground Collisions

The flipping behavior described in Section 2 involves collisions of the front legs with the ground. In order to recover as much of the impact kinetic energy as possible, our controllers position the front leg vertically prior to impact, resulting in the radial compliance of the leg to do most of the work.

In order to derive an accurate model of the collision, it would be possible to extend the continuous dynamics to construct a "stance phase" model that might then be integrated to obtain a more accurate prediction of the body kinetic energy returned at the next leg liftoff event. Examples of such predictive impulse models can be found in the literature [5]. However, the accuracy of such models is still hostage to the difficulty of determining the dynamic properties of materials as well as other unmodeled effects [3, 4].

In consequence, we have chosen to incorporate a purely algebraic collision law in our model, where a single coefficient of restitution summarizes the incremental effects of leg compression/decompression. The following assumptions underlie the construction of our collision law[2].

[2]See [9] for details of these assumptions.

A 2 *If a leg is in flight, its angular velocity relative to the body is always zero ($\dot{\phi}_i = 0$), but its position can be arbitrarily specified.*

Accurate modeling of multiple simultaneous collisions is a very fragile and somewhat ill-posed problem [4]. Our flipping controller, due to the very particular sequence of leg placements that it enforces, never encounters multiple simultaneous collisions.

A 3 *Multiple simultaneous collisions are not allowed.*

A 4 *During the collision, we assume that $\tau_i = 0$ and the impulsive foot contact force acts along the leg.*

In situations where our algebraic model violates basic constraints of such collision laws [3], we augment our model to use an incremental approach.

A 5 *If the leg touches the ground outside the friction cone (i.e. $|\tan(\theta + \phi_i)| > \mu$), then the leg immediately starts slipping and transitions into stance without any impulsive collisions. The system velocities remain continuous ($\dot{\theta}^+ = \dot{\theta}^-$).*

Under these assumptions, our collision law models the damping losses arising from the compression and decompression of the front leg as well as the additional thrust provided by the middle and back legs. We assume that these losses can be lumped into a single coefficient of restitution $-1 \leq k_r(\gamma_c)$ as a function of the toe angle at the onset of collision, γ_c.

$$\dot{\theta}^+ = -k_r(\gamma_c)\ \dot{\theta}^- \tag{9}$$

4 An Improved Controller

4.1 Constraints on the Control Inputs

Given a particular contact state p, ground reaction forces on the toes can be determined using (3). Similarly, we can compute the contact force on the tail,

$$F_c^z = \begin{bmatrix} -p^T & Md\cos\theta \end{bmatrix} \mathbf{v_p}(\mathbf{q}, \boldsymbol{\tau}) + Mg - Md\sin\theta\ \dot{\theta}^2 \ .$$

To preserve consistency with the assumed contact state in a physically realistic way, all of these ground reaction forces must be positive, limiting the set of input torque vectors. The following definition captures these constraints and the practical torque limits.

Definition 4 *For a particular state $\mathbf{q} \in T\mathcal{Q}$ and a contact state $p \in \mathcal{H}_l$, we define the set of allowable torques, $\mathcal{T}(\mathbf{q}, p)$ as the set of all torque input vectors $\boldsymbol{\tau} \in \mathbb{R}^3$ such that*

$$\begin{aligned} F_c^z(\mathbf{q}, \boldsymbol{\tau}, p) &\geq 0 \\ \forall i,\ F_i(\mathbf{q}, \boldsymbol{\tau}, p) &\geq 0 \\ \forall i,\ |\tau_i| &\leq \tau_{max} \end{aligned}$$

4.2 Maximal Thrust Control

The vector field (7) is a continuous function of the state and the input torques. As a consequence, the problem of choosing hip controls to maximize the thrust becomes a constrained optimization problem over the allowable input torque space. However, this optimization problem is computationally demanding due to the nonlinearity arising from discrete changes in the contact states. Fortunately, in each of the distinct leg contact states, the optimization problem is linear in the control input torques. Hence, the problem decomposes into a small number of separate linear programming problems, from whose independent solutions may be derived a single correct torque value for the three hips. More formally, given a leg contact state vector, $p \in \mathcal{H}_l$, we pose the corresponding linear programming problem for that region of configuration state space:

$$\begin{aligned} \boldsymbol{\tau}_M(\mathbf{q}, p) &:= \underset{\boldsymbol{\tau}\ \in\ \mathcal{T}(\mathbf{q},p)}{\operatorname{argmax}} \left(\ddot{\theta}(\mathbf{q}, \boldsymbol{\tau}, p) \right) \\ \ddot{\theta}_M(\mathbf{q}, p) &:= \ddot{\theta}(\mathbf{q}, \boldsymbol{\tau}_M(\mathbf{q}, p), p) \ . \end{aligned}$$

The set of contact state assignments that we need to consider is determined by the kinematic constraints, $\mathcal{P}_\mathbf{q} := \{p \in \mathcal{H}_l \mid s_c(\theta) \geq p\}$. The solution to the global problem then becomes,

$$\begin{aligned} \boldsymbol{\tau} &= \boldsymbol{\tau}(\mathbf{q}, p_{max}) \\ p_{max} &:= \underset{p\ \in\ \mathcal{P}_\mathbf{q}}{\operatorname{argmax}} \left(\ddot{\theta}_M(\mathbf{q}, p) \right) \ . \end{aligned} \tag{10}$$

Note that p_{max} is also maximal at the current body state and with the torque solution to the above optimization problem as a result of Lemma 1. Consequently, the actual contact state determined by the algorithm of Section 3.5 will necessarily match p_{max}, that is

$$s_m(\mathbf{q}, \boldsymbol{\tau}(\mathbf{q}, p_{max})) = p_{max} \ .$$

4.3 Hybrid Energy Pumping

Depending on the frictional properties of the surface, our maximal thrust controller may not be enough to complete the flip in one shot. In these cases, our controller uses the hybrid strategy of Section 2, repeatedly applying maximal thrust following each collision.

Currently, we have very little analytical understanding of the behavior arising from this hybrid controller. As a consequence, we only explore in simulation the flipping behavior and its dependence on various surface parameters in the following sections.

5 Simulations

5.1 Apex Return Maps

Following each thrust cycle, the body either flips over, or the body angle reaches a highest point and starts falling back. In presenting the properties of the hybrid pumping strategy, we will find it useful to sample the θ trajectory at this apex point during each cycle. This results in a one dimensional return map, characterizing the behavior of the energy pumping strategy under the maximal thrust actuation. This section explores this return map on the basis of numerical simulation. Formal analysis of this model is presently in progress.

Figure 3 illustrates different types of return maps resulting from different choices of the surface parameters μ, k_c and k_d. This collection of return maps appears to capture all the possible types of phenomena that arise from our hybrid controller.

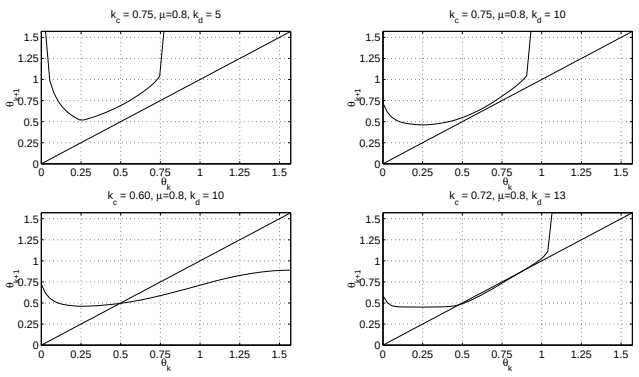

Figure 3: The predicted range of physical behaviors based upon numerical return maps computed for (7) with representative surface parameter settings using the maximal thrust feedback controller (10).

The upper left case has low ground friction and hence the initial thrust is sufficient to flip the robot body over. In contrast, the upper right case has enough friction to make flipping in one thrust impossible, but still has no fixed point, yielding successful flipping after several hops. The remaining cases, unlike the previous ones, have stable fixed points, trapping the robot at a small angle. For the bottom left case, there is no other fixed point, making it impossible for the robot to flip. The bottom right case, however, also has another unstable fixed point, making a successful flip possible for certain initial conditions.

5.2 Maximal Thrust vs PD Control

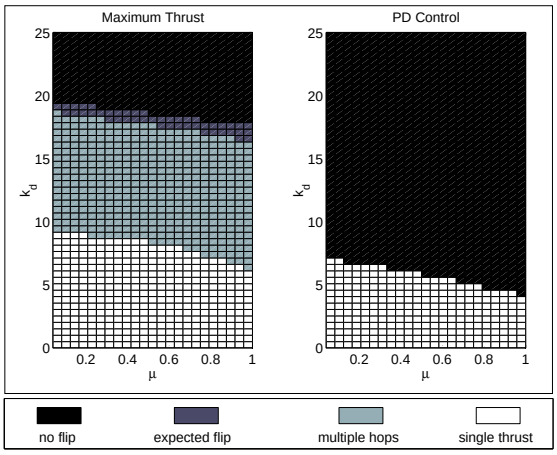

Figure 4: Outcomes for flipping attempts with lower coefficient of restitution, $k_c = 0.75$

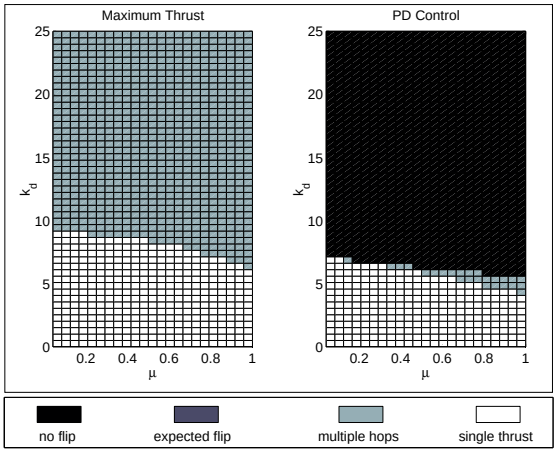

Figure 5: Outcomes for flipping attempts with higher coefficient of restitution, $k_c = 0.9$

Simulation runs for a range of surface friction parameters are illustrated in Figures 4 and 5, for $k_c = 0.75$ and $k_c = 0.9$, respectively. The simulations were run over a range of surface friction properties, until either the robot flipped over or at the end of 50 hops. A particular attempt was considered a success if the body angle reached $\pi/2$ before termination, (labeled *single thrust* and *multiple hops* in the plots), or the sequence of apex heights kept increasing even in the last hops (

labeled *expected flip* in the plots). All other runs were considered failures.

One of the reasons for the choice of such high coefficients of restitution is the active nature of the collisions. They reflect the additional thrust exerted by the back and middle legs during the decompression of the front leg. On RHex, we observed the duration of the collision to be significant, increasing the effect of this active phase of the collision. The actual coefficients, however, still remain to be experimentally verified.

These results demonstrate that maximal thrust control yields considerably better flipping performance than the PD control in all cases. For smaller k_c, where the "active" collision is not properly modeled, the PD controller never succeeds with multiple hops and only has a chance when the first thrust is sufficient. When the effects of the active collision are incorporated through the coefficient of restitution, the maximal thrust controller is still successful in a very large range of surface conditions and yields strictly better results than the PD control.

6 Conclusion and Future Work

In robotic locomotion research, autonomy is likely to impose some of the most demanding constraints on design and limitations on behavior. It is very difficult, often impossible to achieve in systems otherwise designed for non-autonomous operation. RHex, our hexapedal platform, demonstrated that autonomy as a design goal can achieve significant advances in real world performance and robustness.

In this paper, we present a new controller to implement self-righting behavior on RHex, which is perhaps the simplest instance of self-manipulation other than locomotion itself. Our modeling and analysis yields significant improvements to the simple first generation controller, extending its domain of success to a wider range of terrain conditions — between three to five times the range (in regard to the effective viscous damping that can be overcome). Although the implementation of these improvements on our experimental platform awaits a more complete sensory suite, we believe the actual performance improvement on the robot will be comparable to what we have observed in simulation.

More formal analysis of the preliminary model we have described in this paper is also of great interest. Extensions of the flipping behavior such as uninterrupted rolling or handstands will require a much better analytical understanding of the model as well as modifications such as relaxing the friction constraint on the body. We believe that, such extensions to the behavioral suite of a morphology as limited as RHex, is the best way to address the shortcomings of contemporary actuation and energy storage technology while continuing to press ahead in the development of practically useful robots.

Acknowledgments

This work was supported in part by DARPA/ONR Grant N00014-98-1-0747.

References

[1] RHex: A Biologically Inspired Hexapod Runner. *Autonomous Robots*, 11:207–213, 2001.

[2] J. E. Bares and D. S. Wettergreen. Dante II: Technical Description, Results and Lessons Learned. *International journal of Robotics Research*, 18(7):1–29, July 1999.

[3] A. Chatterjee. *Rigid Body Collisions: Some General Considerations, New Collision Laws, and Some Experimental Data*. PhD thesis, Cornell University, 1997.

[4] A. Chatterjee and A. Ruina. A new algebraic rigid body collision law based on impulse space considerations. *journal of Applied Mechnanics*, 65(4):894–900, December 1998.

[5] W. Goldsmith. *Impact: The theory and physical behavior of colliding solids*. Edward Arnold, Ltd., London, 1960.

[6] E. Hale, N. Schara, J. W. Burdick, and P. Fiorini. A Minimally Actuated Hopping Rover for Exploration of Celestial Bodies. In *Proceedings of the IEEE International Conference On Robotics and Automation*, pages 420–7, San Francisco, CA, April 2000.

[7] L. Matthies et al. A Portable, Autonomous, Urban Reconnaissance Robot. In *Proceedings of The 6th International Conference on Intelligent Autonomous Systems*, Venice, Italy, July 2000.

[8] U. Saranli, M. Buehler, and D. E. Koditschek. RHex: A Simple and Highly Mobile Robot. *International journal of Robotics Research*, 20(7):616–631, July 2001.

[9] U. Saranli and D. E. Koditschek. Design and Analysis of a Flipping Controller for RHex. Technical Report CSE-TR-452-02, UM, Ann Arbor, MI, 2001.

[10] E. Tunstel. Evolution of Autonomous Self-Righting Behaviors for Articulated Nanorovers. In *Proceedings of the 5th International Symposium on Artificial Intelligence, Robotics and Automation in Space*, pages 341–6, Noordwijk, The Netherlands, June 1999.